Video Article

Synthesis and Catalytic Performance of Gold Intercalated in the Walls of Mesoporous Silica

Yazhou Ji[1], Christopher Caskey[1], Ryan M. Richards[1]

[1]Department of Chemistry and Geochemistry, Colorado School of Mines

Correspondence to: Ryan M. Richards at rrichard@mines.edu

URL: https://www.jove.com/video/52349
DOI: doi:10.3791/52349

Keywords: Chemistry, Issue 101, Gold, intercalated, silica, mesoporous material, nano reactor, thermally stable, catalyst, recyclable

Date Published: 7/9/2015

Citation: Ji, Y., Caskey, C., Richards, R.M. Synthesis and Catalytic Performance of Gold Intercalated in the Walls of Mesoporous Silica. *J. Vis. Exp.* (101), e52349, doi:10.3791/52349 (2015).

Abstract

As a promising catalytically active nano reactor, gold nanoparticles intercalated in mesoporous silica (GMS) were successfully synthesized and properties of the materials were investigated. We used a one pot sol-gel approach to intercalate gold nano particles in the walls of mesoporous silica. To start with the synthesis, P123 was used as template to form micelles. Then TESPTS was used as a surface modification agent to intercalate gold nano particles. Following this process, TEOS was added in as a silica source which underwent a polymerization process in acid environment. After hydrothermal processing and calcination, the final product was acquired. Several techniques were utilized to characterize the porosity, morphology and structure of the gold intercalated mesoporous silica. The results showed a stable structure of mesoporous silica after gold intercalation. Through the oxidation of benzyl alcohol as a benchmark reaction, the GMS materials showed high selectivity and recyclability.

Video Link

The video component of this article can be found at https://www.jove.com/video/52349/

Introduction

As an emerging technology that has great potential in catalysis applications, nanoscale materials have received intensive research interest in the past decades. Amongst the nanoscale catalysts reported, noble metal catalysts such as Au, Ag, Pd and Pt have attracted world-wide attention [1-3]. Select catalytic reactions include the oxidation of carbon monoxide researchers on Au, Heck reaction on Pd catalysts, and water splitting with Pt. In spite of the promising catalytic potential, nanoscale gold is limited in its applicability due to deactivation from poisoning, coking, thermal degradation, and sintering. It has been reported that gold, as a representative for noble metals, has high selectivity and is less prone to metal leaching, over-oxidation, and self-poisoning[4]. However, the catalytic performance of gold strongly depends on the particle size. Haruta *et al.* has reported the relationship between catalytic performance and gold cluster diameter, demonstrating the highest activity of gold catalysts with particle size ~ 2.7 nm[5].

The particle size of noble metals can be controlled by the preparation method[6-9]; however, the major hindrance towards broad application remains aggregation and loss of activity. To solve the problem of sintering, a common method is to immobilize nanoscale particles on a support material. Various support materials have been applied including porous silica[10-11], semiconducting metal oxides[12-13], polymers[14], graphene[15] and carbon nanotubes[16]. Amongst the materials used, porous silica is an attractive material as a support because it is only mildly acidic, relatively inert, thermally and chemically stable, and can be prepared with very well defined meso-/micro-porosity. The porous structure provides good support for metal particles but also imparts size selective substrate access to the metal catalysts. This selectivity is particularly promising because of the tunability associated with these porous materials. Often, gold particles are found to be extremely mobile on silica surfaces[17-18] and readily form very large (50+ nm) unreactive particles when exposed to high temperatures, thus making it difficult to prepare gold nanoparticles on silica[19]. Mukherjee *et al.* reported immobilization of monodispersed gold nanoparticles on mesoporous silica MCM-41 by 3-aminopropyl-trimethoxysilane and 3-mercaptopropyl-triethoxysilane, and the supported gold nanoparticles were found to be highly active for hydrogenation reactions and no leaching of gold was found in the reaction[20].

Following the report of surface modification of mesoporous silica, we reported a method to prepare gold intercalated into the wall of mesoporous silica (GMS). Additionally, the mesoporous silica supported approach offers a scalable approach to potentially independently alter the catalyst and porous environment. Since catalytic processes are of vital economic importance, the benefits could be far reaching. The ability to develop “green” catalysts would have a profound positive impact on the environment and improve the economic feasibility and resource efficiency of important industrial processes.

Protocol

1. Preparation of GMS

1. Use all chemicals in the following process as received.
2. Prepare 75 ml of 2 M of hydrochloric acid (HCl) solution. Weigh 2.0 g of poly(ethylene glycol)-block-poly(propylene glycol)-block-poly(ethylene glycol) (P123, MW = 5,800) and transfer into the prepared 75 ml of 2 M HCl solution. At RT, apply magnetic stirring to the solution at a speed of 350 r/min until P123 is completely dissolved. The solution will be clear.
3. Weigh 4 g of tetraethoxysilane (TEOS, MW = 208.33) in a small vial and transfer 180 µl of Bis[3-(triethoxysilyl)propyl]-tetrasulfide (TESPTS, MW = 538.94) into the vial. Slowly shake the vial to mix the two chemicals. In another vial, weigh 38 mg of chloroauric acid ($HAuCl_4$, 99.90%) and dissolve in 1 ml of DI water.
4. Increase the P123 solution temperature to 35 °C in an oil bath with temperature controlled by thermocouple.
5. Add all of the mixture of TEOS and TESPTS prepared in step 1.3 to the P123 solution, and keep the solution at vigorous magnetic stirring of 700 r/min. Keep the solution stirring for 2 min, then add all of $HAuCl_4$ solution prepared in step 1.3 dropwise within 30 sec.
6. Keep the solution stirring at 700 r/min for 24 hr at 35 °C.
7. After 24 hr, transfer the solution into a sealed bottle and store in an oven set at 100 °C for 72 hr. This is called hydrothermal processing.
8. After the hydrothermal processing, filter the solution with a #1 filtration paper and negative pressure under a funnel, then wash with water two times and ethanol three times to remove remaining HCl. During each wash process, add water or ethanol 1 cm above solid and wait for the material to dry.
9. Transfer precipitation from filtration to a ceramic crucible and calcine at 550 °C for 4 hr. Set the ramp program as follows: 25 °C to 550 °C for 2 hr, keep at 550 °C for 4 hr, then allow the sample to remain in furnace with the door closed until the temperature falls below 40 °C.
10. After calcination, transfer the product to a glass vial with a plastic spatula. The synthesized material has a red color.

2. Catalytic Reaction, Oxidation of Benzyl Alcohol

1. Since the oxidation of benzyl alcohol is a liquid phase reaction without a separate solvent, measure 5 ml of benzyl alcohol (99.8%) and transfer it into a 25 ml three-neck flask, then weigh 10 mg of GMS catalyst and it add to benzyl alcohol.
2. Set up a temperature-controlled oil bath with magnetic stirring to ensure accurate and uniform control of the reaction temperature.
3. Put the flask with benzyl alcohol and catalyst into the oil bath, then set the temperature to 100 °C and stir at 150 r/min.
4. Flow oxygen gas with 99.9% purity into the flask at 2 ml/min controlled by a mass flow controller.
5. When the temperature of the oil bath reaches 100 °C and stabilizes, introduce oxygen gas into the three neck flask.
6. Keep the oxygen flow rate and temperature constant, and allow the reaction to proceed for 6 hr.
7. After the reaction, filter the product with a #1 filtration paper. Collect the liquid phase and transfer an aliquot to a gas chromatography (GC) vial. In the GC vial, mix four parts HPLC grade acetic acid for every one part sample (For example, use 36 µl sample and 144 µl acetic acid.) Put the vial on a gas chromatograph auto sampler for analysis. Wash off the solid precipitate on the filter paper with DI water and ethanol then allow to dry in air. Collect the dried solid with a spatula as recycled catalyst.
8. Repeat the same experiment procedure from step 2.3 through 2.7 with recycled catalyst three times. In each repeat, adjust the amount of benzyl alcohol to match the ratio described in step 2.2.

3. Thermal Treatment of GMS for Testing of Thermal Stability

1. Weigh three separate 300 mg portions of synthesized GMS, and store them in glass vials. These are marked as batch 1, batch 2 and batch 3. Keep batch 1 as control group, and put batch 2 and batch 3 into a furnace for thermal processing.
2. Program the furnace as follows for processing at 400 °C: ramp from 25 °C to 400 °C in 0.5 hr, maintain at 400 °C for 4 hr, allow the sample to remain in the furnace with the door closed until the temperature falls below 40 °C. Put batch 2 in a crucible and start the program.
3. Program the furnace as follows for processing at 650 °C: ramp from 25 °C to 650 °C in 0.75 hr, maintain at 650 °C for 4 hr, allow the sample to remain in furnace with the door closed until the temperature falls below 40 °C. Put batch 3 in a crucible and start the program.

4. Characterization of GMS Materials[21,22]

1. On the physisorption instrument, degas GMS materials with the following program: 90 °C for 60 min and then 350 °C for 480 min. Run full-isotherm analysis on the degased materials to obtain physisorption data.
2. Disperse GMS sample on a 200-mesh holey carbon TEM grid and observe the sample under a transmission electron microscope. Restrict magnification under 44,000X to protect the material.
3. Run XRD with Cu Kα radiation (λ = 1.5418 Å). Set tube voltage of 45 kV, and tube current of 40 mA. Collect intensity in the 2θ range between 10° and 90° with a step size of 0.008° and a measuring time of 5 sec at each step.

Representative Results

This method was used to compare the levels of heme synthesis in normal (HBEC30KT) vs. cancer (HCC4017) lung cells. **Figure 2** shows a higher level of heme synthesis in cancer cells (HCC4017) than normal lung cells (HBEC30KT). The level of heme synthesis was also measured in normal and cancer cells in the presence of mitochondrial uncoupler carbonyl cyanide 3-chlorophenylhydrazone (CCCP). Cells were treated with 10 µM CCCP for 24 hr before the measurement of heme synthesis levels. As expected, the levels of heme synthesis (**Figure 2**) decreased in the presence of CCCP in both normal and cancer cells. It has been shown previously that heme synthesis can be inhibited by succinyl acetone

(SA), a potent and specific inhibitor of 5-aminolevulinic acid dehydratase (ALAD) which is the second enzyme in heme bio. The synthesized GMS material was characterized by transmission electron microscope (TEM), X-ray diffraction (XRD) and nitrogen physisorption.

As shown in **Figure 1** (batch 1 GMS), images from TEM reveal the structure of mesoporous silica. The silica matrix formed well-defined long channels with stable wall. The pore diameter from TEM was identified to be around 5 nm and hexagonal in the shape as is typical for mesoporous silica. Immobilization of gold nanoparticles was achieved from the synthesis process, as evidenced from the TEM image, there were no gold particles explicitly distributed on the surface or in the mesoporous channel, indicating that the gold particles were successfully intercalated into the walls of mesoporous silica matrix.

To further establish whether the gold particles are intercalated in the walls of the silica matrix, nitrogen physisorption was used. **Figure 2A** is the BET physisorption isotherm for silica matrix without gold intercalation, **Figure 2B** is for GMS with gold intercalated in the walls (batch 1). As seen from the figure, there was no significant difference between the two materials. Both of them showed the typical shape for mesoporous materials with a hysteresis loop. This further indicates the gold intercalation did not impose any alternation on the pore structure (pore size, shape or volume), which taken together with the XRD and TEM (showing the gold is in the form of 4 nm particles) strongly infers that the gold particles are in the walls of silica matrix.

Gold nanoparticles, promising as catalysts, suffer from sintering and loss of activity at elevated temperatures. GMS material synthesized with this method exhibits thermal stability with no aggregation observed after heating. The GMS materials treated at several high temperatures have been characterized by physisorption. **Figure 3A** and **3B** are BET pore structure and BJH pore distribution for GMS material calcined at different temperatures. As indicated in the figure, high temperature calcination did not alter the mesoporous silica matrix. Further, both pore structure and pore distribution remained the same after temperature treatment as high as 650 °C (*i.e.*, the gold did not aggregate and block pores).

The thermal stability of the gold in GMS was further verified by XRD. **Figure 4** is the XRD pattern of GMS material calcined at different temperatures. The two peaks corresponded to Au (110) and Au (111). Peak location, peak intensity and peak width (all indicators of aggregation and particle size) did not show any change due to the calcination process, indicating that gold particles did not change in size or morphology. The high stability is very promising for catalytic reactions at harsh conditions.

Using the oxidation of benzyl alcohol to benzaldehyde as a benchmark, the catalytic properties of GMS were studied. At 100 °C, GMS served as good catalyst for the oxidation reaction. Conversion of benzyl alcohol was 44.1%, and the selectivity of towards benzaldehyde was 92.8%. Recycling experiments of GMS were conducted with the GMS material; the results are shown in **Table 1**. As can be seen from the table, GMS material exhibited good recyclability. For each round of the recycling experiment, the conversion of benzyl alcohol decreased slightly, probably due to small losses of catalyst in transfer. Even after the third time recycling, selectivity remained at a high level, around 90%.

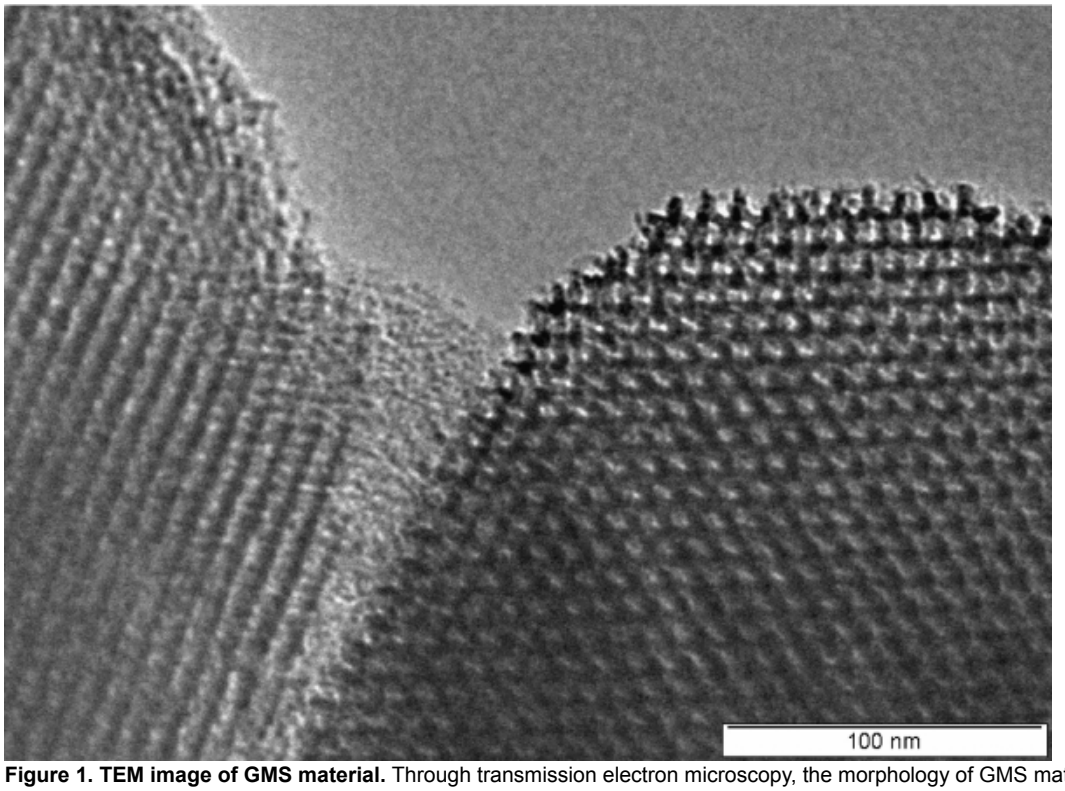

Figure 1. TEM image of GMS material. Through transmission electron microscopy, the morphology of GMS material was observed. Mesoporous silica serves as a matrix for the GMS materials; the structure of mesoporous silica was shown in two different orientations. The TEM image clearly illustrated well-defined long channels and hexagonal pores of mesoporous silica. During the formation of GMS material, the basic structure of the mesoporous matrix was not affected: the pores were not blocked by gold nano particles. Please click here to view a larger version of this figure.

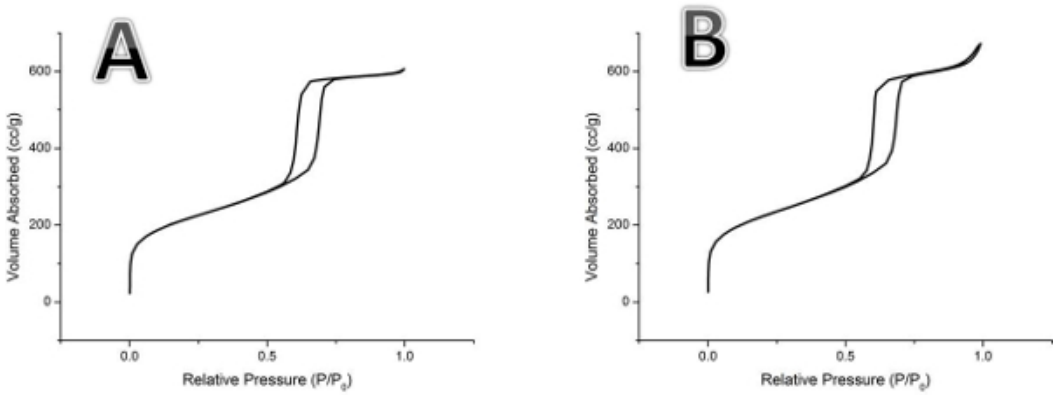

Figure 2. BET pore structure of silica matrix and GMS material. (A) The BET pore structure of mesoporous silica matrix without gold intercalation. **(B)** The BET pore structure of GMS material. Nitrogen physisorption was used to further prove the pore stability. Full isotherm physisorption was performed on GMS material with mesoporous silica as control group. Both the isotherm of mesoporous silica and GMS material showed isotherm with hysteresis loop for typical mesoporous material as defined by IUPAC. The formation of gold nano particles was not blocking the channel nor the pores in the mesoporous matrix. Please click here to view a larger version of this figure.

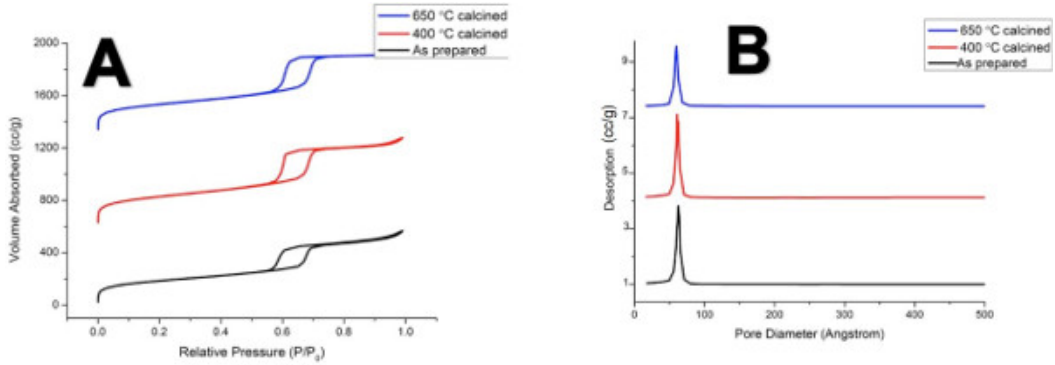

Figure 3. BET pore structure (A) and BJH pore distribution (B) of GMS materials calcined at different high temperatures. Nitrogen physisorption was again used for investigation into thermal stability of GMS materials. Material treated at 400 °C and 650 °C were measured along with the original material which was labeled as as-prepared in the graph. For GMS materials calcined at different temperatures, no changes were observed in isotherm or the BJH pore distribution. The results proved that GMS material was thermally stable at high temperatures, with no structural change in the mesoporous matrix. Please click here to view a larger version of this figure.

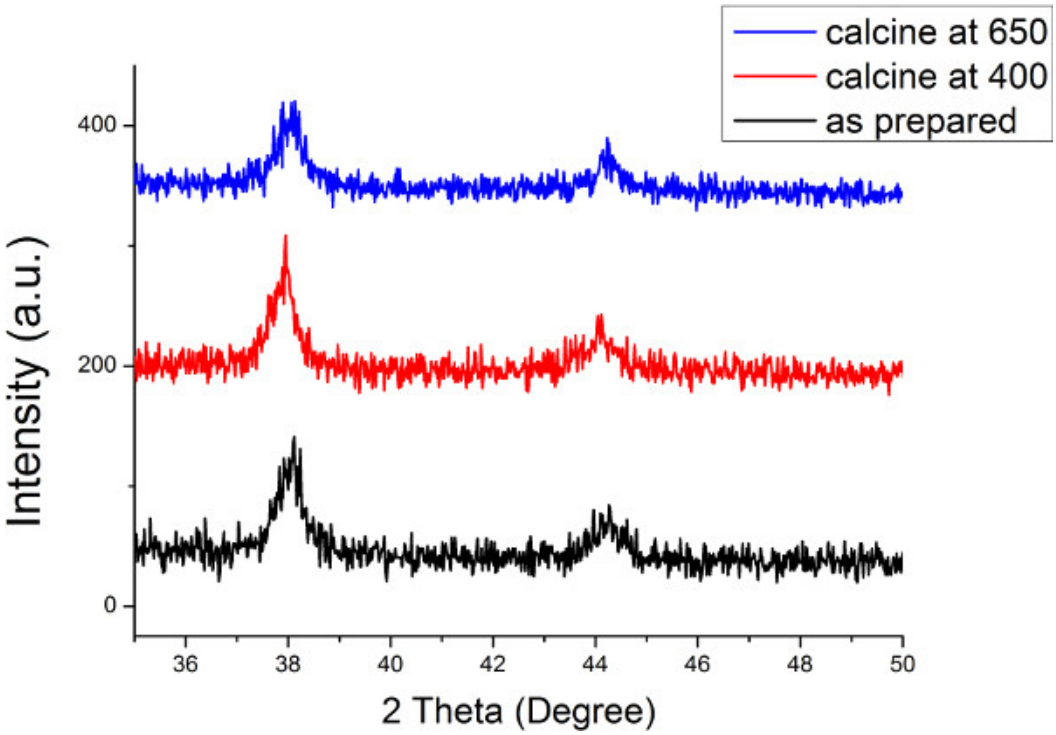

Figure 4. XRD pattern of GMS material calcined at different temperatures. X-ray diffraction was used to show the thermal stability of gold nanoparticles. Materials treated at 400 °C and 650 °C were measured along with original material which was labeled as as-prepared in the graph. During the high temperature calcination, the peak location and peak height of gold nanoparticles did not go through changes, proving that gold nanoparticles did not alter in structure, phase, or morphology. Please click here to view a larger version of this figure.

Table 1. Conversion and selectivity of benzyl alcohol oxidation with GMS recycled three times.

	Conversion of benzyl alcohol (%)	Selectivity of benzaldehyde (%)
GMS 1st cycle	44.1	92.8
GMS 2nd cycle	37.2	89.6
GMS 3rd cycle	35.3	90.1

Discussion

Within the synthesis protocol, attention to surfactant concentration, pH of solution and reaction temperature is critical to the successful formation of GMS. The critical steps are 1.2, 1.3, 1.4 and 1.6. The above mentioned parameters control the critical packing parameter and phase of micelles formed from surfactant. The phase and morphology of micelle determines the final state of silica matrix, which serves as the framework for GMS. Also important in the formation process is the sequence and time to add the HAuCl solution. TEOS and TESPTS act as the silica source and surface modification agent, respectively. Adding the two chemicals first ensures proper polymerization of silica onto micelles and incorporates the sulfur bond into the silica wall, which will further attract gold atoms to form gold nano clusters. Proper sequence and timing ensure the gold particles will be intercalated into the walls of the silica matrix instead of dispersed on the surface.

The synthesis of GMS with this approach provides a new paradigm of immobilizing gold particles in mesoporous silica supports. As GMS exhibits great thermal stability, high catalytic activity and good recyclability, this material is very promising in batch production and application in industrial catalytic process. The successful intercalation of gold is a proof of concept study, with possibility of intercalation of other catalytically active metals under similar protocol. Modifications can be made to this protocol to synthesize AgMS, PtMS and PdMS. The modification procedure can be simply adjusted by changing the metal salt as described in step 1.3. Replace chloroauric acid with corresponding Ag, Pt or Pd salt. Modifications can also be made by altering the gold nano particle size according to reported procedures and following the intercalation procedure[23]. Further expansion of this synthesis method can be made to intercalating facet-controlled metal particles, metal oxides, and nano metal alloys.

This synthesis protocol requires precise control of experimental parameters. In case of failure, troubleshooting can be focused on solution concentration as listed in step 1.2 and 1.3. Carefully monitoring the temperature is also important with particular sensitivity associated with steps 1.4 and 1.6. We have observed that a change of 0.5 °C in solution temperature can result in a failed preparation.

Research efforts have been directed to addressing the challenge of gold particle stability to make robust catalyst for many years. As compared with traditional methods of preparing gold nano particles, such as incipient wetness and direct precipitation, this method to make GMS can

stabilize gold nano particles in the walls framework of silica, thus achieving high levels of durability. The robustness has been confirmed by the thermal stability experiment as described in procedure 3.

Using oxidation of benzyl alcohol as benchmark reaction, the GMS material is proven to be active and recyclable. Application of similar materials (GMS, PtMS, PdMS, *etc.*) can be extended to catalytic processes such as pyrolysis, water splitting and waste disposal, providing a new approach to providing a green and sustainable future.

Disclosures

The authors have nothing to disclose.

Acknowledgements

The authors acknowledge National Science Foundation grant CHE- 1214068 for supporting this research project.

References

1. Furuyama, K., Kaneko, K., Vargas, P. D. Heme as a magnificent molecule with multiple missions: heme determines its own fate and governs cellular homeostasis. *Tohoku J Exp Med.* **213**, 1-16 (2007).
2. Hamza, I., Dailey, H. A. One ring to rule them all: trafficking of heme and heme synthesis intermediates in the metazoans. *Biochim Biophys Acta.* **1823**, 1617-1632 (2012).
3. Zhu, Y., Hon, T., Ye, W., Zhang, L. Heme deficiency interferes with the Ras-mitogen-activated protein kinase signaling pathway and expression of a subset of neuronal genes. *Cell Growth Differ.* **13**, 431-439 (2002).
4. Zhang, L. HEME BIOLOGY: The Secret Life of Heme in Regulating Diverse Biological Processes. *Singapore: World Scientific Publishing Company.* (2011).
5. Mense, S. M., Zhang, L. Heme: a versatile signaling molecule controlling the activities of diverse regulators ranging from transcription factors to MAP kinases. *Cell Res.* **16**, 681-692 (2006).
6. Ingram, D. J., Kendrew, J. C. Orientation of the haem group in myoglobin and its relation to the polypeptide chain direction. *Nature.* **178**, 905-906 (1956).
7. Perutz, M. F. X-ray analysis of hemoglobin. *Science.* **140**, 863-869 (1963).
8. Chance, B. The nature of electron transfer and energy coupling reactions. *FEBS Lett.* **23**, 3-20 (1972).
9. Guengerich, F. P., MacDonald, T. L. Mechanisms of cytochrome P-450 catalysis. *Faseb J.* **4**, 2453-2459 (1990).
10. Igarashi, K., *et al.* Multivalent DNA binding complex generated by small Maf and Bach1 as a possible biochemical basis for beta-globin locus control region complex. *J Biol Chem.* **273**, 11783-11790 (1998).
11. Ogawa, K., *et al.* Heme mediates derepression of Maf recognition element through direct binding to transcription repressor Bach1. *Embo J.* **20**, 2835-2843 (2001).
12. Oyake, T., *et al.* Bach proteins belong to a novel family of BTB-basic leucine zipper transcription factors that interact with MafK and regulate transcription through the NF-E2 site. *Mol Cell Biol.* **16**, 6083-6095 (1996).
13. Snyder, S. H., Jaffrey, S. R., Zakhary, R. Nitric oxide and carbon monoxide: parallel roles as neural messengers. *Brain Res Brain Res Rev.* **26**, 167-175 (1998).
14. Sun, J., *et al.* Hemoprotein Bach1 regulates enhancer availability of heme oxygenase-1 gene. *Embo J.* **21**, 5216-5224 (2002).
15. Zhang, L., Guarente, L. Heme binds to a short sequence that serves a regulatory function in diverse proteins. *Embo J.* **14**, 313-320 (1995).
16. Hon, T., Lee, H. C., Hu, Z., Iyer, V. R., Zhang, L. The heme activator protein Hap1 represses transcription by a heme-independent mechanism in Saccharomyces cerevisiae. *Genetics.* **169**, 1343-1352 (2005).
17. Chernova, T., *et al.* Neurite degeneration induced by heme deficiency mediated via inhibition of NMDA receptor-dependent extracellular signal-regulated kinase 1/2 activation. *J Neurosci.* **27**, 8475-8485 (2007).
18. Chernova, T., *et al.* Early failure of N-methyl-D-aspartate receptors and deficient spine formation induced by reduction of regulatory heme in neurons. *Mol Pharmacol.* **79**, 844-854 (2011).
19. Sengupta, A., Hon, T., Zhang, L. Heme deficiency suppresses the expression of key neuronal genes and causes neuronal cell death. *Brain Res Mol Brain Res.* **137**, 23-30 (2005).
20. Smith, A. G., Raven, E. L., Chernova, T. The regulatory role of heme in neurons. *Metallomics.* **3**, 955-962 (2011).
21. Raghuram, S., *et al.* Identification of heme as the ligand for the orphan nuclear receptors REV-ERBalpha and REV-ERBbeta. *Nat Struct Mol Biol.* **14**, 1207-1213 (2007).
22. Wu, N., Yin, L., Hanniman, E. A., Joshi, S., Lazar, M. A. Negative feedback maintenance of heme homeostasis by its receptor Rev-erbalpha. *Genes Dev.* **23**, 2201-2209 (2009).
23. Yin, L., *et al.* Rev-erbalpha, a heme sensor that coordinates metabolic and circadian pathways. *Science.* **318**, 1786-1789 (2007).
24. Zhu, Y., Hon, T., Zhang, L. Heme initiates changes in the expression of a wide array of genes during the early erythroid differentiation stage. *Biochemical and biophysical research communications.* **258**, 87-93 (1999).
25. Yao, X., Balamurugan, P., Arvey, A., Leslie, C., Zhang, L. Heme controls the regulation of protein tyrosine kinases Jak2 and Src. *Biochemical and biophysical research communications.* **402**, 30-35 (2010).
26. Ye, W., Zhang, L. Heme controls the expression of cell cycle regulators and cell growth in HeLa cells. *Biochem and biophys res comm.* **315**, 546-554 (2004).
27. Hooda, J., Shah, A., Zhang, L. Heme, an essential nutrient from dietary proteins, critically impacts diverse physiological and pathological processes. *Nutrients.* **6**, 1080-1102 (2014).
28. Hooda, J., *et al.* Enhanced heme function and mitochondrial respiration promote the progression of lung cancer cells. *PloS one.* **8**, e63402 (2013).

29. Atamna, H., Walter, P. B., Ames, B. N. The role of heme and iron-sulfur clusters in mitochondrial biogenesis, maintenance, and decay with age. *Arch Biochem Biophys.* **397**, 345-353 (2002).
30. Atamna, H., Killilea, D. W., Killilea, A. N., Ames, B. N. Heme deficiency may be a factor in the mitochondrial and neuronal decay of aging. *Proc Natl Acad Sci U S A.* **99**, 14807-14812 (2002).
31. Ponka, P. Cell biology of heme. *Am J Med Sci.* **318**, 241-256 (1999).
32. Brawer, J. R., Naftolin, F., Martin, J., Sonnenschein, C. Effects of a single injection of estradiol valerate on the hypothalamic arcuate nucleus and on reproductive function in the female rat. *Endocrinol.* **103**, 501-512 (1978).
33. Daniell, W. E., *et al.* Environmental chemical exposures and disturbances of heme synthesis. *Environ Health Perspect.* **105**, Suppl 1. 37-53 (1997).
34. Kihara, T., *et al.* Hepatic heme metabolism in rats with fever induced by interleukin 1beta. *Res Commun Mol Pathol Pharmacol.* **104**, 115-126 (1999).
35. Vijayasarathy, C., Damle, S., Prabu, S. K., Otto, C. M., Avadhani, N. G. Adaptive changes in the expression of nuclear and mitochondrial encoded subunits of cytochrome c oxidase and the catalytic activity during hypoxia. *Eur J Biochem.* **270**, 871-879 (2003).
36. Anderson, K. E. S. S., Bishop, D. F., Desnick, R. J. Disorders of heme biosynthesis: X-linked sideroblastic anemia and the porphyrias. *The Metabolic and Molecular Bases of Inherited Disease.* 1-53 The McGraw-Hill Companies, Inc New York (2009).
37. Salvo, M. L., Contestabile, R., Paiardini, A., Maras, B. Glycine consumption and mitochondrial serine hydroxymethyltransferase in cancer cells: the heme connection. *Med Hypotheses.* **80**, 633-636 (2013).
38. Ishii, D. N., Maniatis, G. M. Haemin promotes rapid neurite outgrowth in cultured mouse neuroblastoma cells. *Nature.* **274**, 372-374 (1978).
39. Padmanaban, G., Venkateswar, V., Rangarajan, P. N. Haem as a multifunctional regulator. *Trends Biochem Sci.* **14**, 492-496 (1989).
40. Rutherford, T. R., Clegg, J. B., Weatherall, D. J. K562 human leukaemic cells synthesise embryonic haemoglobin in response to haemin. *Nature.* **280**, 164-165 (1979).
41. Ye, W., Zhang, L. Heme deficiency causes apoptosis but does not increase ROS generation in HeLa cells. *Biochemical and biophysical research communications.* **319**, 1065-1071 (2004).
42. Bonkovsky, H. L., *et al.* High-performance liquid chromatographic separation and quantitation of tetrapyrroles from biological materials. *Anal Biochem.* **155**, 56-64 (1986).
43. Sinclair, P. R., Gorman, N., Jacobs, J. M. Measurement of heme concentration. *Curr Protoc Toxicol.* **8**, Unit 8.3 (2001).
44. Barros, M. H., Carlson, C. G., Glerum, D. M., Tzagoloff, A. Involvement of mitochondrial ferredoxin and Cox15p in hydroxylation of heme O. *FEBS Lett.* **492**, 133-138 (2001).
45. Shinjyo, N., Kita, K. Up-regulation of heme biosynthesis during differentiation of Neuro2a cells. *J Biochem.* **139**, 373-381 (2006).
46. Israels, L. G., Yoda, B., Schacter, B. A. Heme binding and its possible significance in heme movement and availability in the cell. *Ann N Y Acad Sci.* **244**, 651-661 (1975).
47. Yannoni, C. Z., Robinson, S. H. Early-labelled haem in erythroid and hepatic cells. *Nature.* **258**, 330-331 (1975).
48. Robinson, S. H. Formation of bilirubin from erythroid and nonerythroid sources. *Semin Hematol.* **9**, 43-53 (1972).
49. Granick, S., Granick, D. Nucleolar necklaces in chick embryo myoblasts formed by lack of arginine. *J Cell Biol.* **51**, 636-642 (1971).
50. Morell, D. B., Barrett, J., Clezy, P. S. The prosthetic group of cytochrome oxidase. 1. Purification as porphyrin alpha and conversion into haemin alpha. *Biochem J.* **78**, 793-797 (1961).
51. Sinclair, P., Gibbs, A. H., Sinclair, J. F., de Matteis, F. Formation of cobalt protoporphyrin in the liver of rats. A mechanism for the inhibition of liver haem biosynthesis by inorganic cobalt. *Biochem J.* **178**, 529-538 (1979).
52. Chung, J., Haile, D. J., Wessling-Resnick, M. Copper-induced ferroportin-1 expression in J774 macrophages is associated with increased iron efflux. *Proc Natl Acad Sci U S A.* **101**, 2700-2705 (2004).

